Annular Modes and their Climate Impacts in the GFDL Coupled Ocean-Atmosphere Model

Alex Hall and Martin Visbeck
Lamont-Doherty Earth Observatory
of Columbia University
PO Box 1000, 61 Route 9W
Palisades, NY 10964-8000

contact information:
Alex Hall
Tel: (914) 365-8875
FAX: (914) 365-8736
e-mail: alexhall@rosie.ldeo.columbia.edu

submitted to *Journal of Climate*

Abstract

In the first part of this paper, we characterize the wintertime 'annular modes' in an 800 year integration of the GFDL R15 coupled ocean-atmosphere model. In both hemispheres, the first EOF of surface pressure is almost perfectly described as an oscillation of mass between mid and high latitudes. However, in the northern hemisphere (NH), the mid-latitude mass distribution associated with the annular mode is concentrated in lobes over the North Atlantic and Pacific, while in the southern hemisphere (SH), the distribution is nearly zonally symmetric. In the NH, the annular mode is also biased toward the Atlantic sector, with the most coherent out-of-phase pressure relationship occurring between Iceland and the Azores, while in the SH, the bias toward any particular longitude is weaker. The SH annular mode is therefore more 'annular' than its NH counterpart. In these respects the simulated annular modes are similar to the observed annular modes, except that the Pacific lobe of the simulated NH mode is too intense. The spectra of the NH and SH annular modes indices are white. They also show that both NH and SH annular modes have approximately the same total variance.

In the second part, we examine the simulated climate impacts of the SH annular mode. Compared to the NH, the surface air temperature anomalies associated with the SH annular mode are small. However, the strong geostrophic winds implied by the circular pole-centered pressure pattern of the annular mode have significant implications for the ocean. When the annular mode is in a positive phase (analogous arguments apply for the negative phase), these winds induce a northward Ekman current in the upper layer of the circumpolar ocean. This Ekman pumping explains most of the variability of the circumpolar current's meridional component. Through mass conservation, this circulation leads to upwelling near the edge of the Antarctica, and downwelling just north of the circumpolar current, accounting for much of the upwelling variability in this region. By altering the meridional temperature gradient, these upwelling and downwelling anomalies lead to variations in the intensity of the circumpolar current; for time scales shorter than 50 years, the correlation between the SH annular mode index and the total transport across the Drake Passage is 0.8. Finally, the Ekman pumping advects sea ice away from Antarctica, resulting in thinner sea ice around the continent, and thicker ice closer to the ice margin. Because the ice thickness pattern associated with the annular mode is so ring-like, the annular

mode accounts for most of the variability in total areal coverage of sea ice; for time scales longer than 10 years, the correlation between the SH annular mode index and ice coverage is 0.6.

1 Introduction

Enough measurements exist to characterize the dominant mode of variability poleward of 20° in both the northern and southern hemispheres (NH and SH): it can be roughly described as an oscillation of mass between mid and high latitudes. The teleconnection between mid and high latitude pressure was first recognized in the North Atlantic sector of the NH, where measurements are relatively plentiful. Walker and Bliss (1924), analyzing North Atlantic temperature and pressure data, coined the term 'North Atlantic Oscillation' (NAO) to describe the out-of-phase relationship between pressure over the Azores and Iceland. Armed with better observations, Kutzbach (1970) and Wallace and Gutzler (1981) also examined and quantified this teleconnection. One theme of all these studies is that the dominant mode of variability is best identified by the most prominent teleconnection (i.e. the two points where the pressure anti-correlation is largest). These two points lie in the Atlantic sector. More recently, empirical orthogonal function (EOF) analysis has become a basis for identifying modes of variability. This technique, which identifies the mode that accounts for the most overall variability, is highlighted in papers by Thompson and Wallace (Thompson and Wallace 1998 and Thompson and Wallace 1999). They found that the first EOF of the pressure field has a ring-like structure, with pressure in both the Atlantic and Pacific sectors out-of-phase with pressure over the Arctic. In addition, they analyzed SH data, and showed that an analogous, nearly zonally symmetric pressure oscillation between mid and high latitudes exists there. Because this ring-like structure is present in both hemispheres, they proposed the term 'annular mode' to describe the dominant mode of variability in mid to high latitudes. We will rely on this definition throughout this paper.

In this study, we analyze the behavior of annular modes in a long-term integration of the GFDL coarse resolution coupled ocean-atmosphere model (described in section 2). One of our aims is to explore how physical understanding of the dominant mode of simulated variability in both hemispheres is influenced by analysis

technique. Thus we will compare results based on the most prominent surface pressure teleconnection to results based on EOF analysis of the surface pressure field. To test the limits of the annular mode concept, we also wish to examine the picture that emerges by assuming that the dominant mode of variability is perfectly annular. Thus we will use the zonal-mean pressure difference between mid and high latitudes to define an index of annular mode variability. In total, we will have three methods to examine the annular modes. It turns out that physical understanding is enhanced by examining results from all three techniques together, allowing us to arrive at a unified picture of the annular modes, including a comparison of the modes' behavior in the northern and southern hemispheres. This portion of our study is presented in section 3. Then, in section 4, we examine the simulated climate impacts of the annular modes. Since this issue is relatively well-understood for the dominant mode of variability in the NH, we will focus on the climate impacts of the SH annular mode.

Relatively little has been written about the behavior of annular modes in models. This is unfortunate, since a physically-based numerical model of the climate can complement understanding based on observations nicely. First, it can provide long time series that are much more stable and reliable in a statistical sense than observational time series. Second, it provides global data coverage. To study the SH annular mode, this is especially useful because of sparsity of measurements in the SH poleward of 30°S. The fact that we are using a model that includes an oceanic component is also helpful; as we will show, the SH annular mode has interesting and potentially significant oceanographic implications. At the present time, adequate ocean observations are not readily available to address this issue.

2 Model Description

The most important features of this model are described in some detail in Manabe et al. (1991). It consists of a general circulation model of the ocean coupled to an atmospheric general circulation model through exchange of heat, water, and momentum. The variables of the nine-vertical-level atmospheric component are represented in the horizontal by a series of spherical harmonics (rhomboidal truncation at zonal wavenumber 15) and corresponding grid point values (7.5° longitude by about 4.5° latitude gridbox size). The radiative transfer calculation includes a seasonal cycle

of insolation, but no diurnal cycle. In addition, it takes into account the effects of clouds, water vapor, carbon dioxide, and ozone on incoming and outgoing radiation, though only water vapor and clouds are predicted by the model's dynamical components. At the land surface, the model computes budgets of snow, water, and heat. Soil moisture is parameterized using a 'bucket' model. The finite-difference oceanic component, with a horizontal resolution of 4.5° latitude by 3.75° longitude and 12 vertical levels, uses the Modular Ocean Model (MOM) code described in Pacanowski et al. (1991). This particular version of MOM is based, in turn, on a model described by Bryan and Lewis (1979). In addition to horizontal and vertical background sub-grid scale mixing, the model has isopycnal mixing as discussed by Redi (1982) and Tziperman and Bryan (1993). Convection occurs whenever the vertical stratification becomes unstable. Sea ice is predicted using a free drift model developed by Bryan (1969).

To prevent rapid climate drift that could distort the internal variability this study seeks to diagnose, the fluxes of heat and water obtained from the atmospheric component are modified by given amounts before they are imposed upon the ocean surface. While these 'flux corrections' vary seasonally and geographically, they do not vary from year to year. Therefore they are unlikely to amplify or damp anomalies of sea surface salinity or temperature in a systematic way. Although the adjustments do not eliminate the shortcomings of the model (Marotzke and Stone 1995), they do prevent rapid drift of the simulated climate from realistic initial conditions.

Eight hundred years of detrended model data were used for this study. Since the annular modes are strongest in winter, wintertime averages of all variables were taken prior to analysis. Thus all information we present pertaining to the NH is based on averages over DJF, while all information pertaining to the SH is based on JJA averages.

3 Simulated Annular Modes

As discussed in section 1, one of our aims is to use alternative methods of defining the dominant mode of wintertime variability at mid to high latitudes to characterize the annular modes. To analyze the teleconnection pattern of the annular modes, we identified the two points in both the NH and SH where the surface pressure anti-

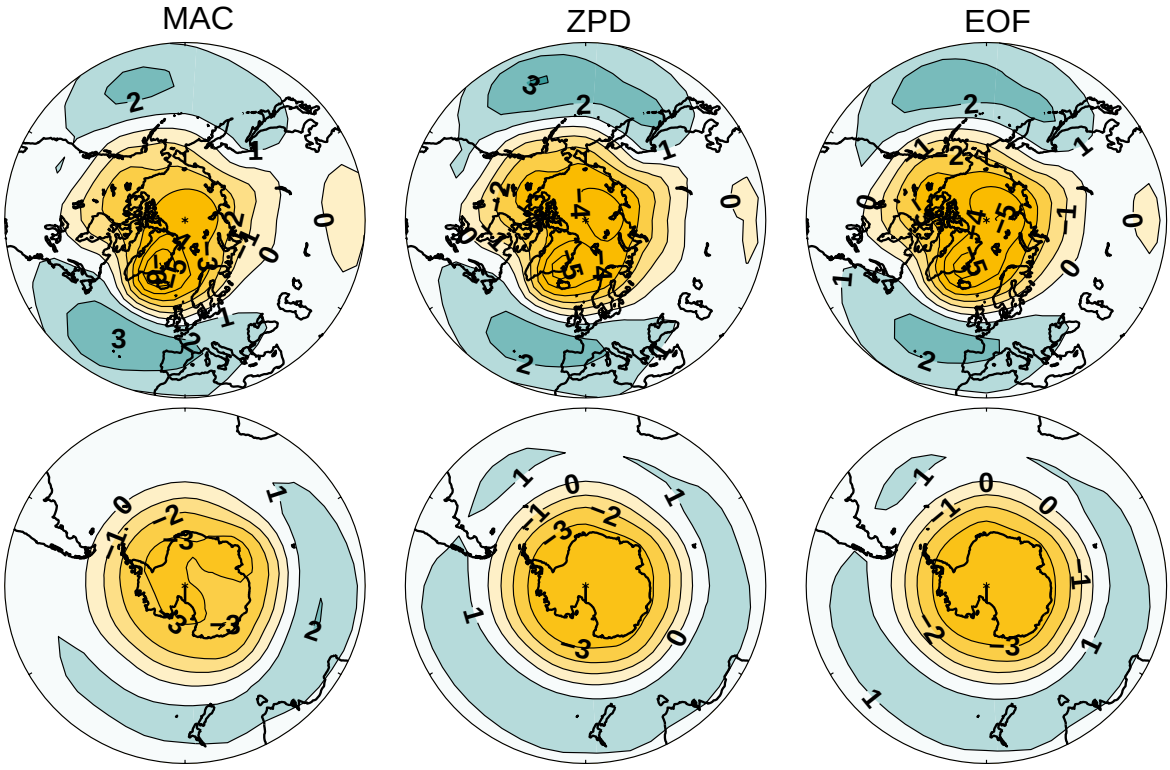

Figure 1: The pressure patterns associated with the MAC, ZPD, and EOF indices. Units are hPa. Model geography is suppressed to facilitate orientation.

correlation is largest. These points are centered on 70°N, 26°W and 38°N, 34°W in the NH, and 70°S, 56°E and 38°S, 101°E in the SH. Note that the latitudes of these points are the same in both hemispheres. An index was then defined as the surface pressure difference between the low and high latitude points. This index will be identified throughout this paper as the Maximum Anti-Correlation (MAC) index. To create the index measuring the zonally symmetric aspect of the annular modes, we calculated the zonal-mean surface pressure difference at the latitudes where the points defining the MAC index are located (70° and 38°). This index is will be identified as the Zonal-mean Pressure Difference (ZPD) index. Finally, the index that captures the most pressure variability was defined as the time series associated with the first EOF of wintertime surface pressure (EOF index). Pressure data over the entire hemisphere was used to calculate the EOF.

Figure 1 shows the pressure patterns associated with the MAC, ZPD and

EOF indices. In the case of the MAC and ZPD indices, these patterns are given by the regression of local surface pressure onto the indices. Before the regressions were calculated, the MAC and ZPD time series were normalized so that their variances were equal to one. The EOF pattern is simply the first EOF of the surface pressure field. The EOF time series automatically has unit variance, so that all pressure patterns represent the typical local pressure anomaly associated with one standard deviation fluctuation of the index in question.

The pressure patterns associated with the three indices are similar for both hemispheres; all show an 'annular' pattern with low pressure at the poles and high pressure at mid-latitudes. Moreover, the ZPD and EOF patterns are nearly identical for both hemispheres. Thus the zonal mean pressure gradient almost perfectly captures the dominant mode of variability as given by the first EOF. This implies that the first EOF has the same straightforward physical explanation in both hemispheres: it is almost purely characterized by an oscillation of mass between mid and high latitudes. The MAC pattern, though similar to the EOF pattern, does not match it as well as the ZPD pattern. In particular, the Atlantic sector is represented more strongly in the NH, making the MAC pattern less zonally symmetric than either the ZPD or EOF patterns. In the SH too, annularity is reduced in the MAC pattern, though somewhat less so. The NH MAC pattern is very similar to the classic NAO teleconnection pattern, with low pressure over Iceland, and high pressure over the Azores (see e.g. Wallace and Gutzler (1981)).

The similarities and differences among these pressure patterns aside, they all illustrate an interesting contrast between the annular modes of the two hemispheres: The SH mode is much more annular than its NH counterpart. For example, examining the EOF pattern, the isolines of pressure at high-latitudes are nearly circular in the SH, whereas they are more wave-like in the NH. In addition, virtually all of the mid-latitude signal in the NH is concentrated in the Atlantic and Pacific sectors, with very little signal over land. In the SH, on the other hand, pressure is anomalously high nearly everywhere in mid-latitudes when pressure is low over the pole. Thus the NH pattern is characterized by Atlantic and Pacific 'lobes', while the SH pattern is characterized by a simple ring. At the same time, the magnitudes of the pressure anomalies of the NH lobes are about twice as large as the mid-latitude pressure anomalies of the SH ring. Since the NH lobes cover approximately half of the total

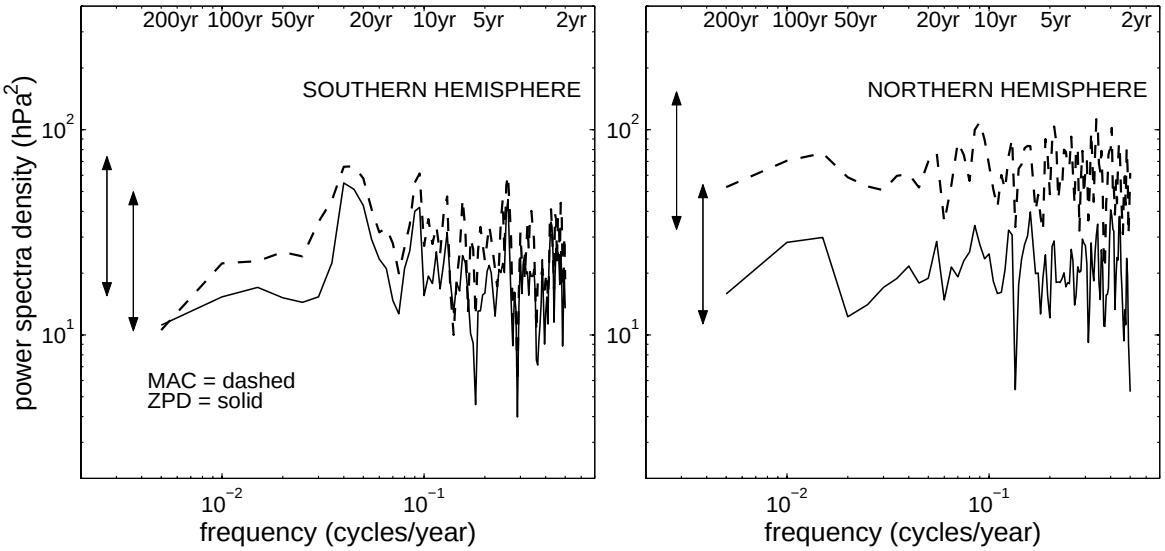

Figure 2: Spectra of MAC and ZPD annular mode indices, calculated using the multi-taper method. The arrows represent the limits within which 95% of the points lie for a white noise time series with the same variance. Time scales are labeled at the top of the plot.

area of the mid-latitudes, the total atmospheric mass redistribution associated with a one standard deviation anomaly of the EOF (or ZPD) index is approximately the same in both hemispheres. Interestingly, the total variance accounted for by the first EOF is also approximately the same in both hemispheres (NH=52.7%, SH=52.8%). Thus the annular modes account for about half the pressure field variability in both hemispheres.

The NH and SH EOF patterns of figure 1 are qualitatively similar to the observed patterns, as documented in figure 1 of Thompson and Wallace (1999), which shows the first EOF of the observed geopotential height field at the lowest levels of the troposphere. Although observations are sparse, the real SH annular mode is quite zonally symmetric, like the model. In the NH, both observed and modeled patterns exhibit obvious zonal asymmetries, with lobes in the Pacific and Atlantic sectors. However, in the observed record, the anomalies of the Pacific lobe are about half as large as the Atlantic lobe, whereas in the model they are approximately equal in magnitude.

Interesting similarities and differences between the NH and SH annular modes are also revealed by examining the spectra of the MAC and ZPD annular mode indices, shown in figure 2. Since the EOF time series are almost perfectly correlated with their ZPD counterparts (SH correlation=0.98, NH=0.95), their spectra are not shown. The spectra of both indices in the NH appear white on time scales longer than two years. The SH spectra are similar in that they are also nearly white, although the broad peaks around 25 years in both SH indices may be significant. The variances of the MAC and ZPD indices agree quite well on all time scales, although the MAC index tends to have slightly more variability. This small difference probably stems from the fact that the MAC index contains some information about noise at smaller spatial scales which are filtered out of the ZPD index. In the northern hemisphere, in contrast, the variances of the two indices do not agree well at all; the variability of the MAC index is about three times larger than that of the ZPD index. The reason for this difference between the hemispheres is rooted in the zonal asymmetry of the pressure pattern associated with the NH annular mode (see figure 1). As noted above, when pressure is anomalously low over the NH pole, high pressure is concentrated in the Atlantic and Pacific lobes, whereas when pressure is low over the SH pole, high pressure is quite uniformly distributed over the mid-latitudes. Thus a pressure anomaly at any SH mid-latitude point tends to reflect quite well the zonal-mean pressure anomaly. This is much less true in the NH; in the case of the NH MAC index, the mid-latitude point is located in the center of the Atlantic lobe, where the pressure anomaly is much larger than the zonal-mean anomaly. This significantly enhances the variance of the MAC index compared to the ZPD.

While figure 2 reveals that the variability of the MAC index is enhanced in the NH, it also shows that the overall level of variability of the ZPD index is about the same in the two hemispheres. Thus the variability of the atmospheric mass re-distribution between mid and high latitudes is approximately the same in both hemispheres, in spite of the zonal asymmetry of the NH mode. This illustrates one of the difficulties in interpreting the variability of the MAC index. Comparing the two MAC spectra, one might be tempted to conclude incorrectly that the NH annular mode is more vigorous than its SH counterpart.

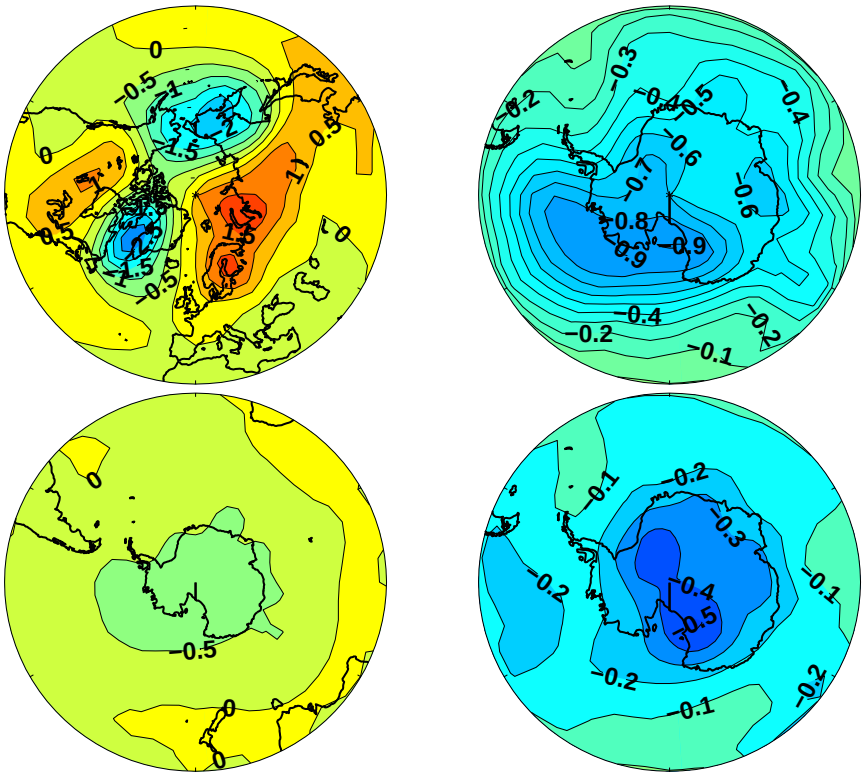

Figure 3: Top left: regression of SAT (°C) onto the time series of the first EOF of the surface pressure field for NH. Bottom left: same as top left (with the same contours) except for the SH. Top right: same as bottom left except for the Antarctic region only (note that contour intervals are also different). Bottom right: same as top right, except correlation between SAT and the EOF time series is shown.

4 Climatic Impacts

In this section, we examine the climate impacts of the annular modes, focusing mainly on the poorly understood SH annular mode, but also incorporating some discussion of the NH for purposes of comparison between the two hemispheres. Throughout this section, we will rely on the EOF index as our annular mode metric. Choice of this index is somewhat arbitrary; however none of the conclusions we present in this section is altered by choosing a different index.

The top left panel of figure 3 shows the regression of surface air temperature

(SAT) onto the EOF index for both hemispheres. The NH case exhibits the familiar NAO pattern of warming over Eurasia, especially northwestern Europe, cooling over Newfoundland and southern Greenland, warming over Canada, and cooling centered over the Bering Sea. It is well-known that this wavenumber two pattern results mainly from the interaction between the counterclockwise geostrophic flow associated with the low over the pole (see figure 1) and the land-sea distribution; warm maritime air is advected over northwestern Europe and Canada, while cold air from the centers of the continents flows to the Bering and Labrador Seas.

The effect of the SH annular mode on SAT is strikingly smaller than in the NH (figure 3, bottom left panel). The main impact is a modest cooling over Antarctica. Why should the impact on SAT be so much smaller in the SH? We have already demonstrated (see figure 2) that the variability of the NH and SH ZPD indices is approximately the same. Thus the magnitudes of the geostrophic wind anomalies must be about the same in both hemispheres. The difference in the SAT impact is due to the relative zonal symmetry of the land-sea (and hence mean temperature) distribution in the SH. Examining the SH EOF pattern of figure 1, it is clear that the most intense geostrophic winds associated with the SH annular mode are located directly over the circumpolar ocean. Unlike the NH case, these winds do not cross from cold land to warm ocean or vice versa, but rather blow continuously across the ocean. Their impact on local SAT is therefore modest.

Since the main impact on SAT is in the Antarctic region, we show a close-up of the SAT regression over Antarctica and the circumpolar ocean in the top right panel of figure 3. The entire Antarctic continent cools more than 0.4°C. The greatest cooling, reaching values of 0.9°C, is centered over the Ross Sea region. These values are roughly in line with the analysis of Thompson and Wallace (see figure 9 of their paper) based on the sparse SAT observations over Antarctica, although the small observed warming over the Antarctic Peninsula does not occur in the model. The values are also similar to those obtained by Fyfe et al. (1999), analyzing the Canadian Climate Coupled Model, although they reported results only for November-April averages (NH winter), rather than during SH winter, when the SH annular mode is most active. To assess the significance of this SAT signal for the climate of the Antarctic region, we calculated the correlation between SAT and the EOF time series, shown in the bottom right panel of figure 3. The correlations are greater in

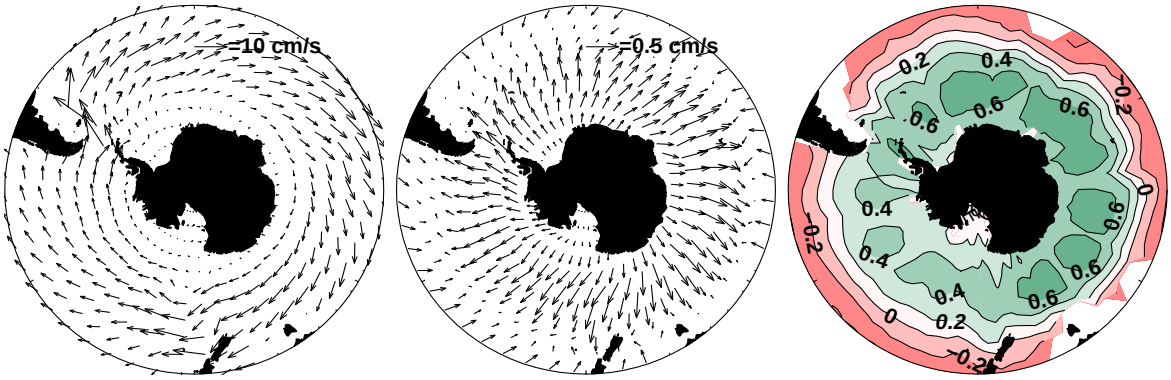

Figure 4: Left: mean JJA currents in the SH ocean poleward of 40°. For clarity, only every other velocity point is plotted. A vector indicating scaling is shown toward the top of the panel. Middle: regression of JJA surface currents onto the time series of the first EOF of the surface pressure field. Note that the scaling vector toward the top of the plot is identical in length to the scaling vector of the left panel but represents a current 20 times smaller in magnitude. Right: correlation between the v-component of the JJA surface current and the EOF time series.

magnitude than 0.3 over most of Antarctica, reaching values of 0.5 over the Ross Sea shelf. Thus although the SH annular mode is a significant contributor to SAT variability in this region, it is clearly not the only source of SAT variability.

While the simulated effects of the SH annular mode on SAT are rather modest compared to the NH, and account for at most a third to a half of SAT variability over Antarctica, the SH annular mode turns out to have significant and interesting effects on the circumpolar ocean circulation. This possibility is readily apparent by examining the pressure pattern of the bottom right panel of figure 1. When the SH annular mode is in its positive phase, clockwise geostrophic flow is driven by the polar low. Because of the nearly-perfect zonal symmetry of the pressure pattern, this creates a nearly uniform zonal wind-stress on the circumpolar ocean. These surface westerlies, in turn, would drive Ekman pumping to the north in the surface layers of the ocean.

To see whether this effect is significant in the model, we analyzed the regression between surface current anomalies and the EOF index, as shown in the middle panel of figure 4. It is clear that the westerly flow associated with a typical posi-

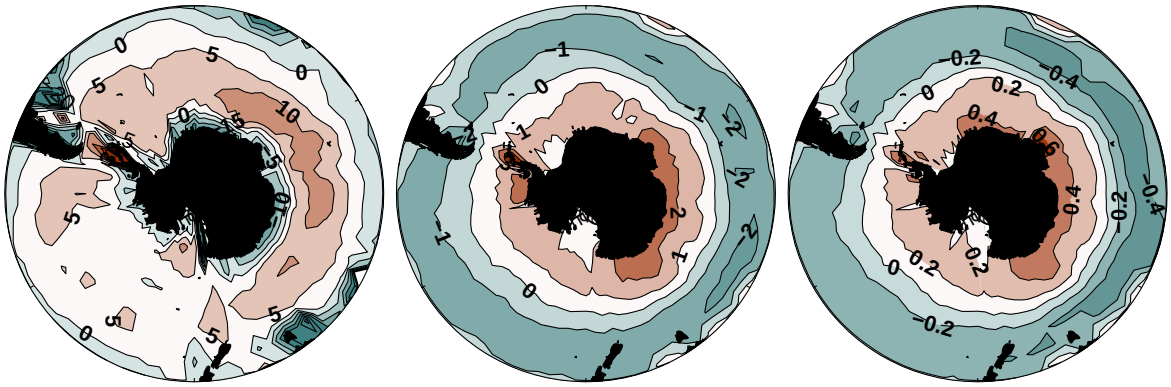

Figure 5: Left: mean JJA upwelling (10^{-7}m/sec) in the SH poleward of 40°. Middle: regression (10^{-7}m/sec) of JJA upwelling onto the time series of the first EOF of the surface pressure field. Right: correlation between JJA upwelling and the EOF time series.

tive excursion of the annular mode index systematically drives a northward Ekman current at all longitudes. Averaged across 61°S, which is about the latitude of the mid-Drake Passage, the magnitude of the northward component of this anomalous current (0.32 cm/sec) is rather large compared to the northward component of the mean current (0.50 cm/sec). Thus a typical positive anomaly of the annular mode increases the northward component of the surface current by more than 60%. Of course, the magnitude of the anomalous northward current is small compared to the mean current speed at this latitude (3.0 cm/sec) whose primary component is the strong eastward flow of the circumpolar ocean (see left panel of figure 4). However, it is large enough to alter significantly the orientation of currents in the Southern Ocean. In addition, the annular mode is the primary mechanism behind fluctuations of the v-component of the circumpolar currents. This is demonstrated by the right panel of figure 4, which shows the correlation between the v-component of the current and the EOF index. The correlations are quite large all around Antarctica, reaching values of 0.6 over much of the Southern Ocean. Thus the annular mode accounts for the lion's share of v-component variability poleward of the tip of South America.

This anomalous northward flow has implications for other aspects of the

ocean circulation. Figure 5 shows the JJA-mean upwelling in the southern ocean (left panel), the regression of JJA upwelling onto the EOF index (middle panel), and finally, the correlation between JJA upwelling and the EOF index (right panel). The mean upwelling field is characterized by downwelling on the order of 5-15 10^{-7}m/sec around the coast of Antarctica, and upwelling of around 5 10^{-7}m/sec throughout the circumpolar ocean. By comparison, the simulated upwelling in the equatorial Pacific, a region where upwelling is particularly intense, averages about 40 10^{-7}m/sec. Thus the typical magnitudes of the upwelling field around Antarctica are not extremely small compared to the rest of the world ocean. A typical positive anomaly of the EOF index drives an upwelling anomaly around the coast of Antarctica on the order of 1-2 10^{-7}m/sec (middle panel). It also drives a zonally-symmetric ring of downwelling of a similar magnitude around the fringes of the circumpolar ocean. Given the horizontal velocity field in the middle panel of figure 4, this vertical circulation is an obvious consequence of mass conservation: The divergent flow around Antarctic must be supplied by upwelling, whereas the convergence at the fringes of the circumpolar ocean must be compensated by downward motion. These upwelling anomalies are rather large (order 20%) compared to the mean values of the upwelling field. Upwelling variability in this region is also well-correlated with the annular mode index (right panel). Correlations between 0.4 and 0.7 are seen around the edges of the Antarctic continent, while anti-correlations less than -0.4 are noticeable in the Indian sector of the circumpolar ocean. Thus not only is the annular mode responsible for upwelling anomalies that are rather large compared to the mean, it also accounts for a great deal of all upwelling variability in this region.

The ocean circulation pattern induced by a positive anomaly of the SH annular mode—upwelling near Antarctica, northward flow across the circumpolar ocean, and downwelling further north—has important implications for the density structure of the Southern Ocean and the associated geostrophic flow. It is well-known that the intense zonal current around Antarctica is sustained by strong meridional temperature (and hence density) gradients. This fact may be understood in terms of the thermal wind relation, whereby a meridional density gradient is associated with a vertical shear of the zonal geostrophic flow. The circulation pattern induced by a positive anomaly of the SH annular mode would intensify the meridional temperature contrast across the circumpolar ocean, mainly by injecting relatively warm surface

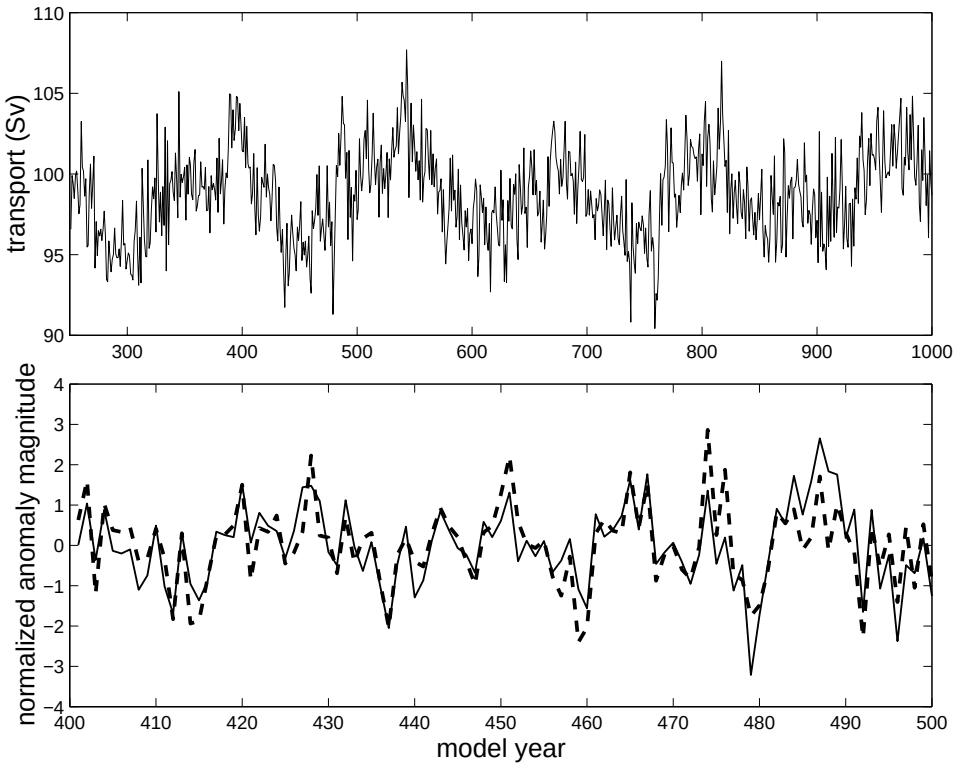

Figure 6: Top panel: Time series of the total JJA transport through the Drake Passage. Bottom panel: Time series of the total transport through the Drake Passage (black) and the EOF index (dashed) for a single century of the simulation. Both time series were filtered using a 50-year high pass filter, then normalized by their standard deviations to facilitate comparison.

waters into the deeper layers at the northern edge of the circumpolar current. This, in turn, would increase the vertical shear—and hence the magnitude—of the zonal geostrophic flow.

Variations in the intensity of the circumpolar current are of great interest to oceanographers. Therefore, to see whether the phenomenon outlined above occurs in the simulation, we created a time series of the total transport across the model's Drake Passage, a measure of the intensity of the circumpolar current. This is shown in the top panel of figure 6. Immediately obvious are large centennial-scale fluctuations in the intensity of the circumpolar current. In addition, large variations on shorter time scales occur. It turns out that the centennial-scale fluctuations, an

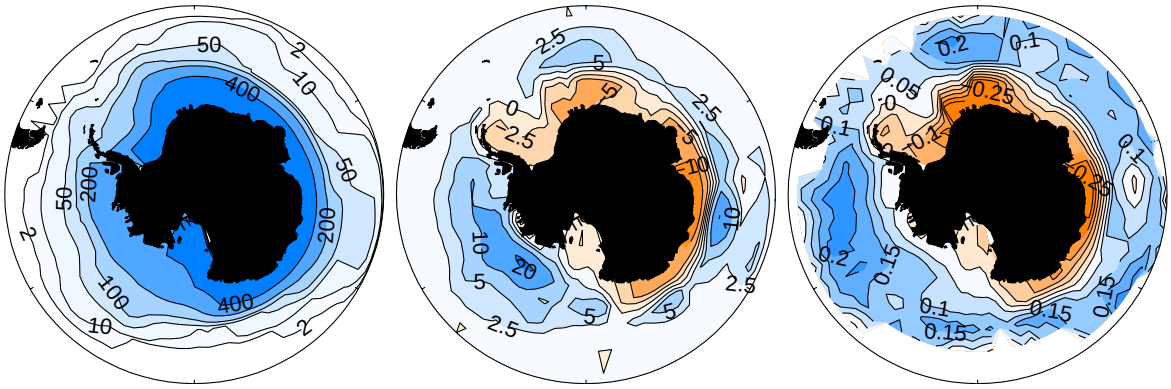

Figure 7: Left: mean JJA sea ice thickness (cm) for the southern ocean poleward of 50°. Middle: regression (cm) of JJA sea ice thickness onto the time series of the first EOF of the surface pressure field. Right: correlation between sea ice thickness and the EOF time series.

analyis of which is beyond the scope of this paper, cannot be related to the SH annular mode. However, the shorter time scale fluctuations can; when the transport and EOF time series are filtered to remove fluctuations longer in time scale than 50 years, the correlation between the two time series is very large–0.81. The very strong relationship between the SH annular mode and variations in the intensity of the circumpolar current is illustrated visually in the bottom panel of figure 6, which shows a blow-up of one century of the 50-year high-pass filtered EOF index and transport time series. Clearly almost all variations in the transport across the Drake Passage shorter in time scale than 50 years can be linked to variations of the SH annular mode. An identical picture emerges by examining other centuries of the simulation. To gage the magnitude of the transport anomaly induced by a fluctuation of the SH annular mode, we calculated the regression of the high-pass filtered transport time series onto the normalized high-pass filtered EOF index: a typical positive anomaly (time scale $\leq$ 50 years) in the SH annular mode is associated with an increase of 1.6 Sv in the transport across the Drake Passage.

The impact of the SH annular mode on sea ice variability is also significant. Figure 7 shows the JJA-mean sea ice field (left panel), the regression of JJA sea ice anomalies onto the SH EOF index (middle), and the correlation between JJA sea ice and the SH EOF index (right). From the middle panel of figure 4, one would

expect the anomalous northward Ekman current associated with the positive phase of the SH annular mode to advect ice away from the Antarctic continent toward the open ocean. The middle panel of figure 7 verifies that this is the case. A decrease in ice thickness on the order of 5 cm is observed around the edges of the continent, while ice thickness increases of about 5 cm occur at lower latitudes. In some areas, notably in the Pacific sector of the circumpolar ocean, the thickness increases are larger, reaching 10-20 cm. While the thickness decreases around the edges of the continent are not large compared to the very large mean ice thickness there (see left panel), the thickness increases over the more thinly covered lower latitudes are large compared to their mean value. For example, following the 10 cm mean thickness contour of the left panel, the thickness anomalies of the middle panel are on the order of 2.5 to 5 cm. The correlations (right panel) between sea ice anomalies and the EOF time series are not large; ice thickness is obviously influenced by thermodynamic processes as well as advection. However, the correlations are systematically arranged in a spatially-coherent, ring-like pattern, with maximum anti-correlation near the continent, and maximum correlation nearer the ice margins. It should be noted that the mean ice thicknesses shown in the left panel of figure 7, are greater than observed: Although the simulated ice thicknesses are constrained to agree with observed values upon coupling, the model climate drifts so that by the end of the integration the thicknesses are somewhat larger than observed. However, this does not affect the conclusions presented here; a more realistic ice field would respond in the same way to the Ekman currents associated with the annular mode.

It turns out that the impact of the annular mode on the variability of sea ice coverage is larger and more significant for low frequencies. Figure 8 shows correlations and regressions between local ice thickness anomalies and the SH EOF index, as in the middle and right panels of figure 7, except that all time series were filtered using a 10 year low-pass filter. Both the correlations and regressions are much larger than in figure 7. The decreases in ice thickness near the Antarctic continent (left panel) are around 10-20 cm, rising to larger than 30 cm in places. The correlations in these regions (right panel) are between -0.2 and -0.5. Typical values of the thickness increase at lower latitudes are also 10-20 cm, though the increase is as large as a half a meter in places. The correlations here also fall between 0.2 and 0.5. In some places, the annular mode accounts for a significant fraction of

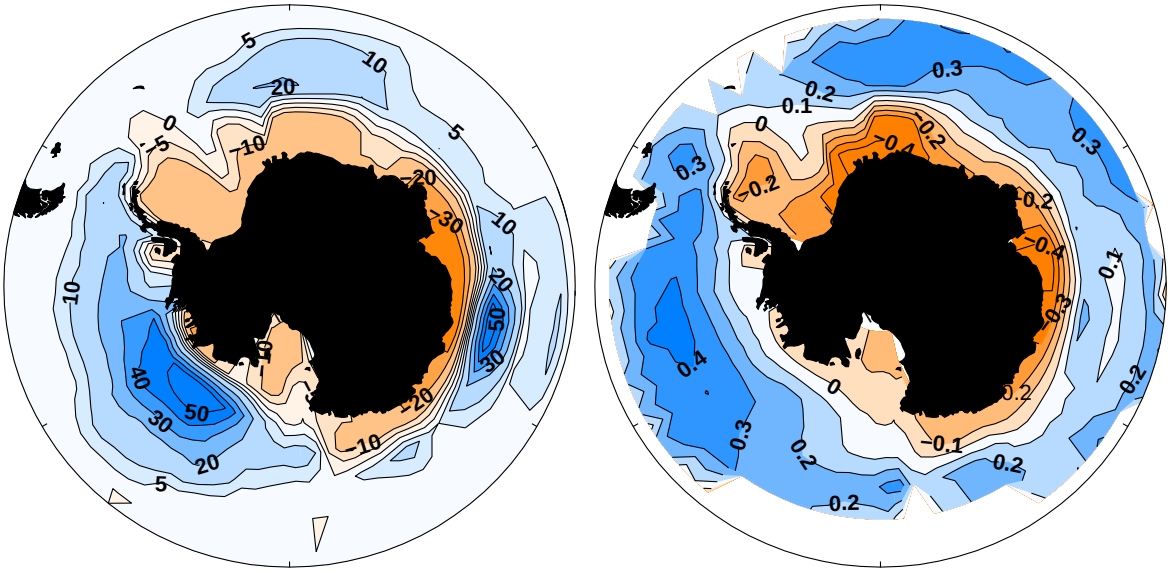

Figure 8: Left: regression (cm) of JJA sea ice thickness onto the time series of the first EOF of the surface pressure field. Right: correlation between sea ice thickness and the EOF time series. All data were filtered to eliminate variability on time scales shorter than 10 years using a Hamming filter.

low-frequency ice thickness variability.

The coherent ring-like pattern of the correlation between local ice anomalies and the EOF time series seen in the right panels of both figures 7 and 8 suggests that the annular mode may have an even more significant role in the variability of the total areal coverage of sea ice, rather than local ice anomalies. Defining the ice margin as the location where the thickness falls below 10 cm, we calculated the correlation between the total area covered by sea ice and the EOF time series. The correlation (0.38) is significantly larger than the correlations seen in figure 7. Just as was the case with local anomalies, most of the correlation between the two time series occurs at low frequencies. In addition, the spectrum (not shown) of the ice coverage time series is quite red, with most of the variability concentrated at time scales longer than 10 years. To focus on these longer time scales, where the correlation is likely to be higher and which contain the lion's share of the ice coverage variability in any case, high-frequency variability was removed from the

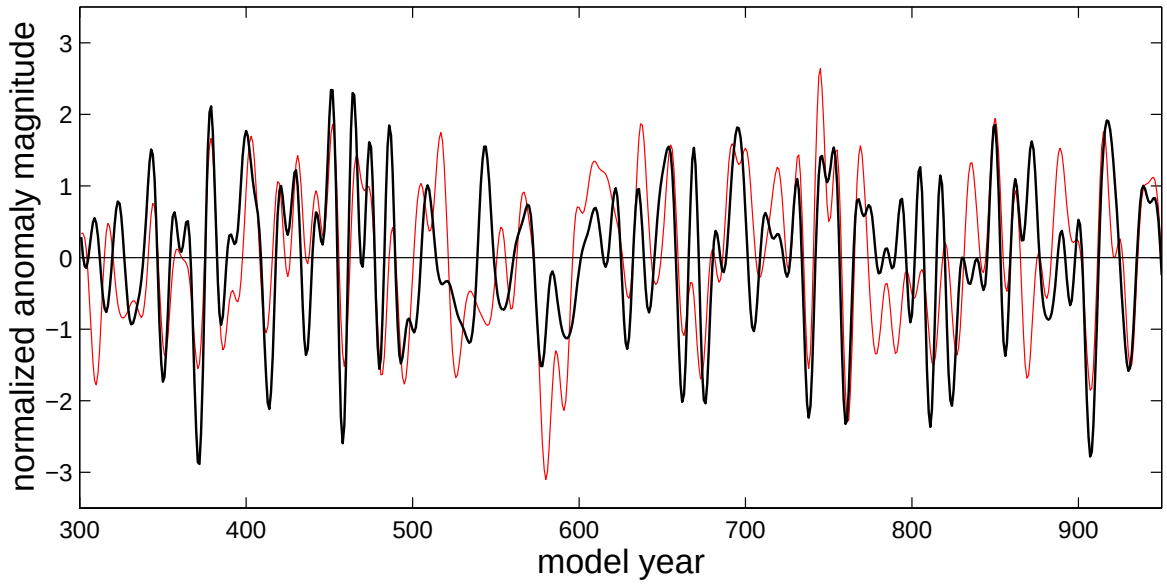

Figure 9: Time series of the SH EOF index (black) and the total area where SH sea ice thickness exceeds 10 cm (red). Both time series were filtered to remove fluctuations shorter in time scale than 10 years. They were also normalized by their standard deviations to allow comparison between the two time series. The entire time series are not shown because of filtering-related data loss. Note that because of the redness of the ice coverage spectrum, the filtered ice coverage time series is very similar to its unfiltered counterpart.

ice coverage and EOF time series using the 10-year low-pass filter. The correlation between the filtered time series is significantly higher—0.6. This strong relationship is illustrated visually in figure 9. The EOF index and ice coverage are in phase at almost all times, with even small fluctuations of the EOF index often mirrored in the ice coverage time series. Thus the SH annular mode accounts for most of the variability of ice coverage in the SH.

To gauge the magnitude of this impact on ice coverage, we regressed the low-pass filtered ice coverage time series onto the low-pass filtered EOF time series. Since we re-normalized the EOF time series after filtering, this represents the sea ice coverage increase that occurs due to a typical low-frequency positive anomaly in the SH annular mode. The value of this regression coefficient is 1.21×10^6 km^2. For

comparison, the total mean JJA sea ice coverage is $2.88 \times 10^7 \text{ km}^2$. Of course, our definition of sea ice margin and hence our measure of sea ice coverage is somewhat arbitrary; however, using other cutoffs gives practically identical answers. This demonstrates that for time scales longer than 10 years, the SH annular mode induces large excursions of the sea ice margin.

5 Summary and Discussion

In section 3, we characterized the wintertime annular modes in this model by examining MAC, ZPD and EOF indices, their associated surface pressure patterns, and their spectra. In both hemispheres, the EOF and ZPD index are almost perfectly correlated and have nearly identical pressure patterns. This indicates that the first EOF of surface pressure is almost perfectly described as an oscillation of mass between mid and high latitudes. However, all three indices show that the mid-latitude pressure distribution of the NH annular mode is concentrated in lobes over the North Atlantic and Pacific, while in the SH, the distribution is nearly zonally symmetric. In addition, in the NH, the most coherent out-of-phase pressure relationship occurs between Iceland and the Azores, while in the SH, the bias toward any particular longitude is weaker. Thus the pressure pattern of the NH MAC index is organized in an NAO-like pattern, with a bias toward the Atlantic sector. For both of these reasons, the SH annular mode is more 'annular' than its NH counterpart. In these respects the simulated annular modes are similar to the observed annular modes, except that the Pacific lobe of the simulated NH mode is too intense. The spectra of the NH and SH annular modes indices are white. They also show that variability in the mass distribution between mid and high latitudes is approximately the same in both hemispheres, in spite of the significant hemispheric differences in the annular mode pressure patterns.

An aquaplanet or a land-only planet would surely have zonally symmetric annular modes at both poles. From this standpoint, the structure of the SH annular mode is easy to understand: the relative zonal symmetry of the land-sea distribution does little to alter the otherwise zonally symmetric annular mode. It is the NH annular mode that is the oddity in need of further explanation. The Atlantic and Pacific lobe pattern of the NH mode is most likely related to the land-sea distribution and the

topography of the land itself. The fact that the most coherent out-of-phase pressure fluctuations occur in the Atlantic sector is probably also related to the land-sea distribution. This lobe pattern, its bias toward the Atlantic sector, and the availability of data led to the concept of the NAO prior to the concept of annular modes. Recently, Deser (2000) challenged the appropriateness of the annular mode concept for the NH, asserting that the dominance of the Atlantic sector in the NH teleconnection patterns favors retaining the NAO concept. Of course, the NAO would not exist if the atmosphere did not have a pre-existing tendency for pressure oscillations between the pole and mid-latitudes (i.e. exhibit 'annular modes'); in this sense, it cannot be considered a phenomenon independent of the NH's annular mode. However, it does seem worthwhile to retain the NAO concept to highlight the anomalous behavior of the NH annular mode. Why it behaves in this eccentric fashion is also a fascinating question for further study. Perhaps the Pacific sector participates less in the NH annular mode because the variability there is more affected by tropical influences, such as the ENSO phenomenon.

In section 4, we examined the poorly-known climate implications of the SH annular mode. Compared to the NH, the SAT anomalies associated with the SH annular mode are small. The difference in the SAT impact is due to the relative zonal symmetry of the land-sea (and hence mean temperature) distribution in the SH. Unlike the NH case, the geostrophic winds implied by the circular pole-centered pressure pattern of the SH annular mode do not cross from cold land to warm ocean or vice versa, but rather blow continuously across the ocean or land. Their impact on local SAT is therefore relatively modest. However, these geostrophic winds do have significant implications for the ocean. When the annular mode is in a positive phase (analogous arguments apply for the negative phase), the surface wind stress induces a northward Ekman current in the upper layer of the circumpolar ocean at all longitudes. This Ekman pumping explains most of the variability of the circumpolar current's meridional component. Through mass conservation, this circulation leads to upwelling near the edge of the Antarctica, and downwelling just north of the circumpolar current, accounting for much of the upwelling variability in this region. By altering the meridional temperature gradient, these upwelling and downwelling anomalies lead directly to variations in the intensity of the circumpolar current; when the variability due to a centennial-scale oscillation unrelated to the SH annular mode

is removed by applying a 50-year high pass filter, the correlation between the SH annular mode index and the total transport across the Drake Passage is 0.8. Finally, this Ekman pumping advects sea ice away from Antarctica, resulting in thinner sea ice around the continent, and thicker ice closer to the ice margin. These anomalies are especially large and significant for variability on time scales longer than 10 years. Because the ice thickness pattern associated with the annular mode is so ring-like, the annular mode accounts for most of the variability in total areal coverage of sea ice; for time scales longer than 10 years, which contain most of the ice coverage variability, the correlation between the SH annular mode index and ice coverage is 0.6. Thus if a long-term trend were to occur in the SH annular mode—whether anthropogenic or natural in origin–this could lead to a trend in the ice margin. Why the SH annular mode does not excite high-frequency excursions of the sea ice margin is an interesting topic for further research.

All of the conclusions presented here regarding the climate impacts of the SH annular mode are for the winter season only. However, unlike its NH counterpart, the SH annular mode only becomes slightly less active during the other seasons in both the real world (see Thompson and Wallace 1999) and the present model. Although a detailed analysis of the climate impacts during other seasons is beyond the scope of this paper, they are likely to be quite similar to those outlined here, with the possible exception of the impact on sea ice, which practically disappears during summertime.

Of course, the resolution of the model used in this study is relatively coarse. However, the simulated SH annular mode is quite realistic and the physical mechanism of the ocean's response—Ekman pumping driving upwelling anomalies and fluctuations of the sea ice margin—is exactly what one would expect based on theoretical understanding of the ocean. It is difficult to see how improved parameterizations or increased resolution would alter this picture in any substantial way. It therefore seems likely that the actual impacts of the SH annular mode on the ocean are qualitatively similar to those seen in this simulation.

Acknowledgments.

Alex Hall is supported by a Lamont Postdoctoral Fellowship. Martin Visbeck is supported by NOAA grant XXXXX.

References

Bryan K (1969) Climate and the ocean circulation: III. The ocean model. *Mon Wea Rev*, 97,806-827.

Bryan K, Lewis L (1979) A water mass model of the world ocean. *J Geophys Res*, 84(C5), 2503-2517.

Deser C (2000) A note on the annularity of the 'Arctic Oscillation'. submitted to *Geophys Res Let*.

Fyfe, JC, Boer GJ, Flato FM (1999) The Arctic and Antarctic Oscillations and the projected changes under global warming. *Geophys Res Let*, 26, 1601-1604.

Kutzbach JE (1970) Large-scale features of monthly-mean northern hemisphere anomaly maps of sea-level pressure. *Mon Wea Rev*, 98:708-716.

Manabe S, Stouffer RJ, Spelman M, Bryan K (1991) Transient responses of a coupled ocean-atmosphere model to gradual changes of atmospheric CO_2. Part I: annual-mean response. *J Clim* 4:785-817

Marotzke J, Stone P (1995) Atmospheric transports, the thermohaline circulation, and flux adjustments in a simple coupled model. *J Phys Oceanogr* 25:1350-1364

Redi MH (1982) Oceanic isopycnal mixing by coordinate rotation. *J Phys Oceanogr*, 12, 1154-1158.

Pacanowski R, Dixon K, Rosati A (1991) The G.F.D.L Modular Ocean Model Users Guide. *GFDL Ocean Group Technical Report 2*

Thompson DWJ, Wallace JM (1998) The Arctic Oscillation signature in the wintertime geopotential height and temperature fields. *Geophys Res Let*, 25:1297-1300.

Thompson DWJ, Wallace JM (1999) Annular Modes in the Extratropical Circulation. Part I: Month-to-month variability. submitted to J Clim.

Tziperman E, Bryan K (1993): Estimating global air-sea fluxes from surface properties and from climatological flux data using an oceanic general circulation model. *J Geophys Res*, 98(C12), 22629-22644.

Walker GT, Bliss EW (1932) World Weather V. *Mem Roy Meteor Soc*, 4:53-84.

Wallace JM, Gutzler DS (1981): Teleconnections in the geopotential height field during Northern Hemisphere winter. *Mon Wea Rev*, 109, 784-812.